Supporting Information

Laser-assisted strain engineering of thin elastomer films to form variable wavy substrates for cell culture.

Caterina Tomba*, Tatiana Petithory, Riccardo Pedron, Aissam Airoudj, Ilaria Di Meglio, Aurélien Roux, Valeriy Luchnikov*

Section 1. Atomic Force Microscopy (AFM) measurements:

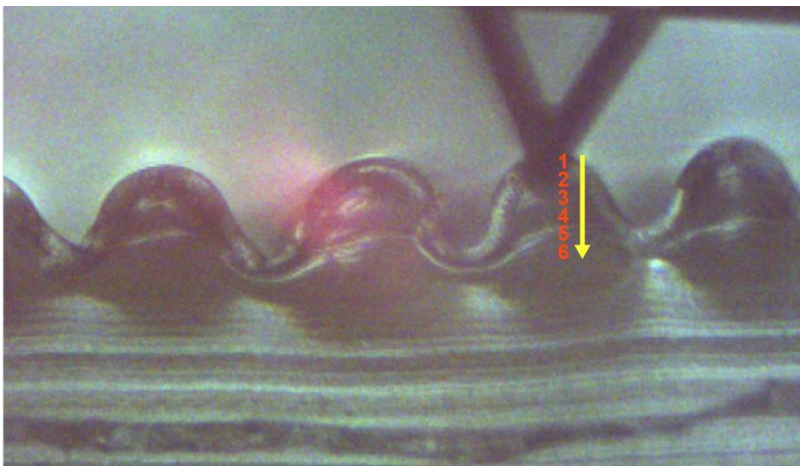

Zone	Young Modulus (MPa)
1	152 ± 11
2	67 ± 8
3	6 ± 2
4	5 ± 3
5	3 ± 1
6	2 ± 1

Figure S1. The AFM measurement scheme and the average Young modulus (mean±s.d.) in the measured zones. FC=20/20/20/100.

AFM measurements were carried out in a Bruker Multimode IV, with a Nanoscope V controller and an E "vertical" scanner, by the Peak Force Quantitative Nanomechanical Mapping (PF-QNM, Bruker) method. In this method, force distance curves are collected by nanoindentation of the sample in a point-by-point mode. During measurement, the maximum (peak force) is controlled at each pixel to obtain force-distance curves which are then used as feedback signal. The loading and unloading force-distance curves are collected at a frequency of 2 kHz at each position within the mapped area of the specimen (Figures S2, S3). In parallel to topography images, information on material elasticity (Young's modulus), tip-to-surface adhesion were obtained. All the experiments were carried out in air and at room temperature. 1 µm x 1 µm (256 x 256 pixels at 0.4 Hz) were taken at several different areas on the sample surface. To get relevant results, the cantilever and the tip geometry are taking into account in the PF-QNM measurements. Thus, a calibration procedure was first followed. All quantitative measurements were carried out with SCANASYST cantilever

(Bruker, USA) with a spring constant of 0.4 N/m and resonance frequency of 70 kHz, a width of 25 μm and a length of 115 μm. Thanks to the Thermal Noise method, the actual spring constant was determined and found to be around 0.33 N/m. Then, the deflection sensitivity (around 29 nm/V) was measured on a sapphire surface. Tip radius was calibrated against a PDMS standard provided by Bruker. The measured value of the tip radius was 15 nm. The Poisson's ratio was assumed to be equal to 0.3. For all experiments, samples were previously (at least half a day before) fixed on a sample holder. The Young modulus, , measured by the Atomic force Microscopy (Peak-Force QNM mode) is estimated to be in the interval of to , while for the untreated film it is . The approximate dependence of the Young modulus on the distance from the surface, shown in Figure S1, implies the existence of the stiffness gradient in the direction normal to the film.

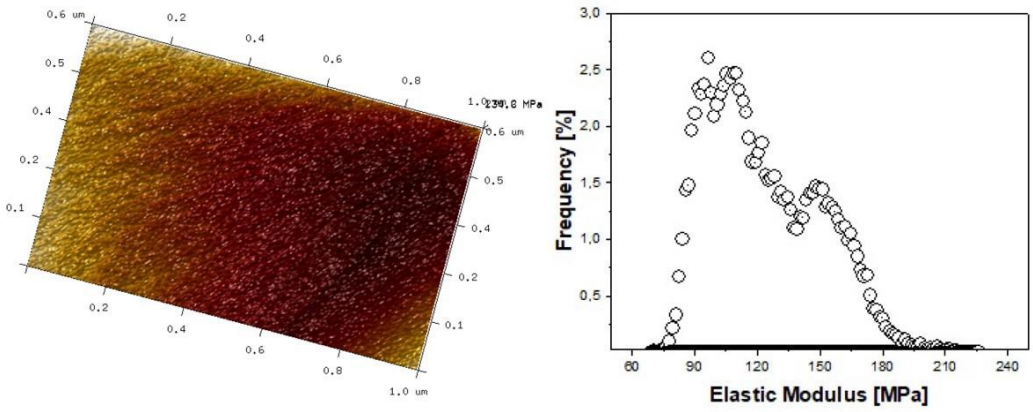

Figure S2. AFM Young modulus mapping (a) and modulus map histogram (b) of the surface layer. FC=20/20/20/100.

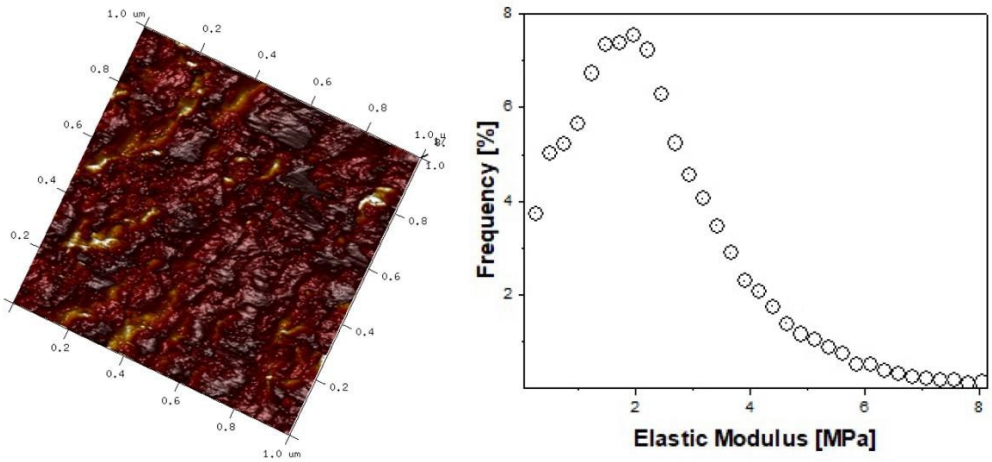

Figure S3. AFM Young modulus mapping (a) and modulus map histogram (b) of the cross-section directly below the *sl/s* interface. FC=20/20/20/100.

Section 2. Stress gradient characterization of the sand-clock shaped substrate:

Deformation of the "sand clock" substrate upon the uniaxial stretching is illustrated by the Figure S4.

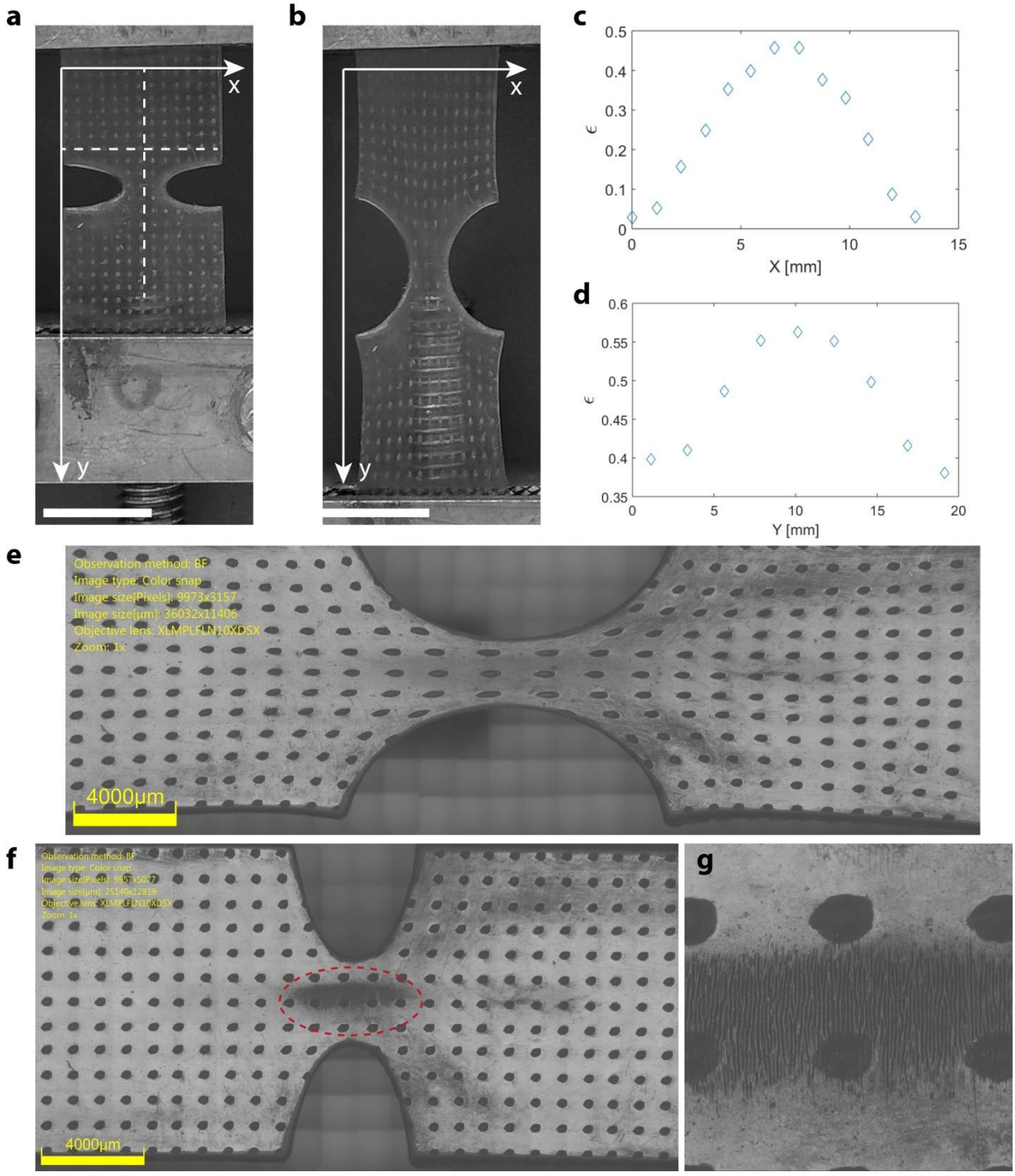

Figure S4. Strain generation in the "sand clock" substrates. a) The initial unstretched substrate. b) The substrate stretched by 56%. c,d) Relative stretching calculated along the vertical and the horizontal dashed lines on the figure (a). Scale bar = 1 cm. e-g) Numerical microscope cartography

of a “sand clock”-shaped substrate, stretched and irradiated by laser. e) Sample stretched by 50%. f) Relaxed sample. g) Wrinkles in the central region, indicated by the red oval on the figure (f).

For this study, the 1mm-thick PDMS films were prepared using the Dow Corning Sylgard 184 Kit, at the standard PDMS :Curing agent ratio 10 :1. Also, we used a commercial silicone substrate (Figures S4e-g). A square array of dots was created on the surface of the substrate by laser engraving.

The shape of the substrate causes the significant gradient of the elongation of the distance between the neighboring points in along the stretching direction, and contraction in the perpendicular direction (the y and x directions on the figure, respectively). We are mostly interested by the elongation deformation, which is responsible for the wrinkles appearing after the laser irradiation and the release of the substrate. Here we characterize this deformation as ( ), where is the distance between the neighboring points in the direction before and after stretching, respectively. Figure S4c represents the value measured along the axial direction marked on the Figure S4a by the vertical dashed line. Due to the specific shape of the substrate, the deformation degree in the narrowest part of the substrate is significantly higher than at the extremities, clamped in the stretching device. The deformation gradient is even more pronounced along the transversal direction, marked by the horizontal dashed line on the Figure S4a. In the present study, we exploit the deformation gradient along the axial line of the substrate, which passes through the « neck » of the sand-clock shaped substrate. In the future studies, we shall try to explore the deformation field numerically, taking into account the complex boundary of the substrate and the nonlinear strain-stress relation of the elastomer.

A more detailed image of the “sand clock”-shaped substrate after elongation by 50% is reported on the Figure S4e. The direction and the magnitude of the elongation of the laser-engraved spots (which are circular for the not stretched substrate, Figure S4f) show the deformation distribution over the sample. Upon laser irradiation of the narrow rectangular region along the horizontal axis of

the sample, the substrate was relaxed, which resulted in the wrinkle formation in the most stretched area (Figure S4g).

Section 3. Raman measurements:

Raman spectra were collected using an Horiba LabRAM 300 Spectrometer using a 532 nm wavelength laser to the sample surface.

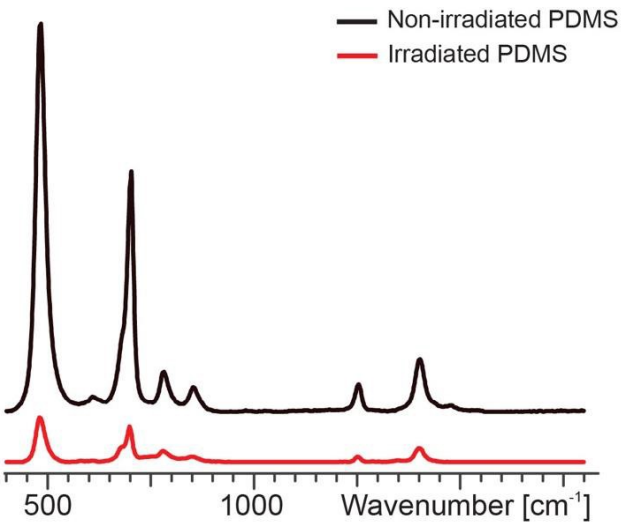

Figure S5. Raman spectra of the non-irradiated and the irradiated PDMS films. The spectrum of the irradiated substrate (FC = 20/20/20/100) are similar to the one of native PDMS. The presence of Si-crystals should have been highlighted by the presence of a sharp peak at 521 cm^{-1} close to the one of the siloxane symmetric stretching at 490 cm^{-1} [1–3].

Section 4. Bistable structures:

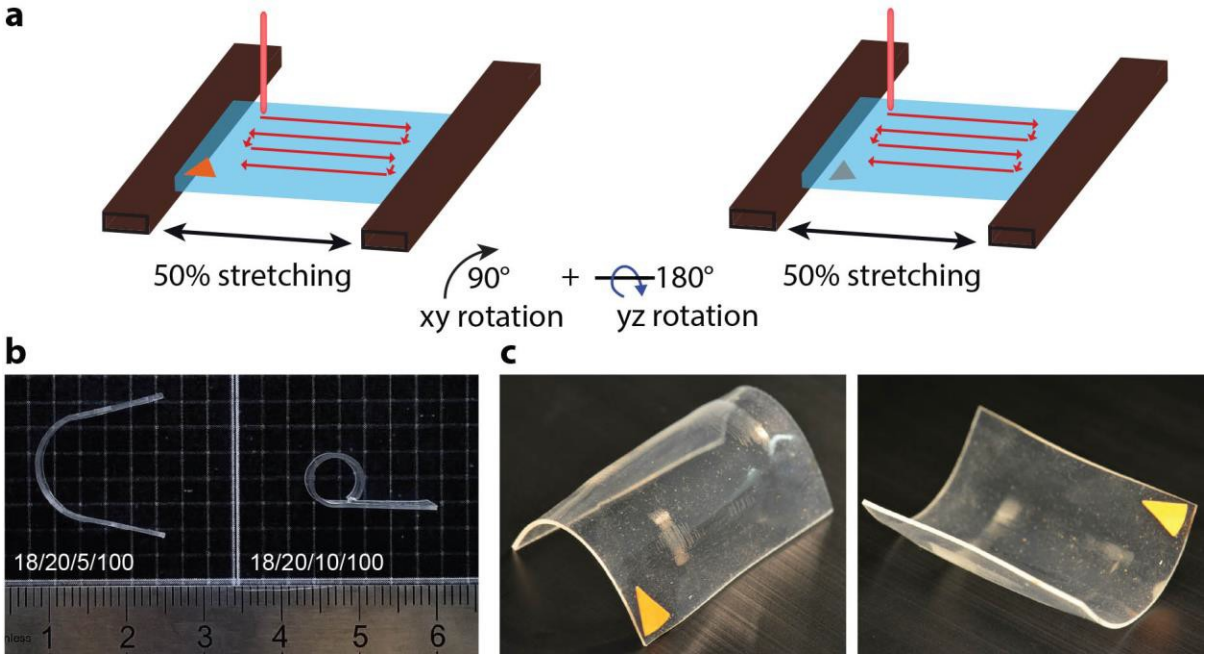

Figure S6. 3D structures apart of the wrinkles. a) Schematic layout of the experimental setup used to produce bistable structures. The PDMS film is successively irradiated on both sides, with a rotation first by 90° around the normal axis, then by 180° around the horizontal axis. b) Bended films, for two different numbers of scans (3 and 10). FC = 18/20/5/100 (left) and 18/20/10/100 (right). Scale unit = 1 mm. c) A bistable structure. FC = 19/20/10/50 for each of the 2 irradiated sides. The triangular mark points towards the cylinder circumference (left picture), whereas it points towards the cylinder axis, once the conformation has been changed (right picture).

Section 5. Cell adaptation to wrinkled patterns on "sand clock"-shaped films:

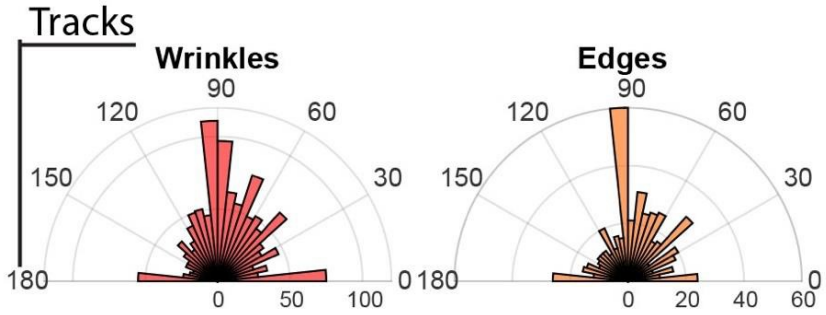

Figure S7. Polar plots of the net track orientation of Hela cells on the "wrinkles" and "edges" regions, without MitomycinC.

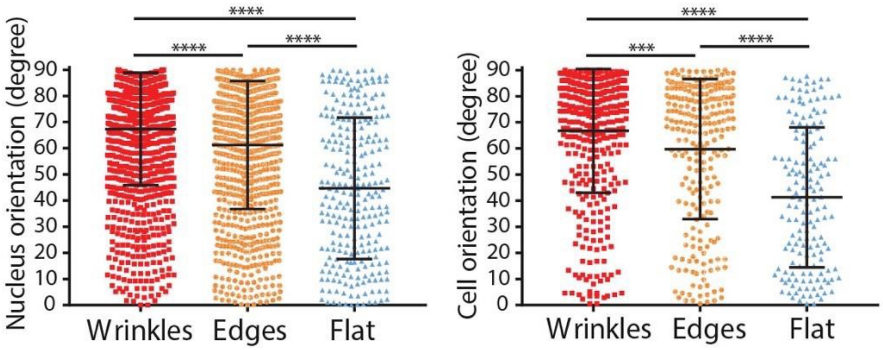

Figure S8. Orientation of nuclei and Hela cells in the 3 regions. Distributions with the mean±s.d. (nuclei, ****, $p < 0.0001$, n=1160, 863, 265; cells, ***, p=0.0004, ****, $p < 0.0001$, n=407, 250, 160, Mann Whitney test).

Section 6. Cell adaptation to stretching of homogeneous wrinkled substrate:

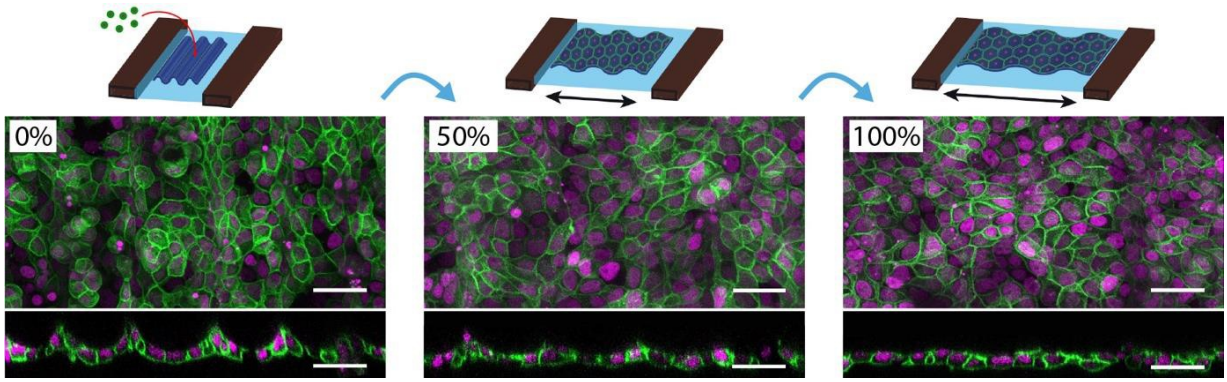

Figure S9. Top views and orthogonal sections of MDCK cells at different rates of substrate stretching: 0% (relaxed), 50% and 100%. Cells are seeded on a relaxed substrate and then stretched to 50% and 100%. Cell membrane (Myr-Palm-GFP, green), nuclei (H2B-mCherry, magenta). Scale bars = 40 μm.

Supplementary references

[1] T. Deschaines, J. Hodkiewicz, P. Henson, *ThermoFisher Appl. Note 51735* **2009**, 3.

[2] P. A. Atanasov, N. E. Stankova, N. N. Nedyalkov, N. Fukata, D. Hirsch, B. Rauschenbach, S. Amoruso, X. Wang, K. N. Kolev, E. I. Valova, J. S. Georgieva, S. A. Armyanov, *Appl. Surf. Sci.* **2016**, *374*, 229.

[3] N. E. Stankova, P. A. Atanasov, R. G. Nikov, R. G. Nikov, N. N. Nedyalkov, T. R. Stoyanchov, N. Fukata, K. N. Kolev, E. I. Valova, J. S. Georgieva, S. A. Armyanov, *Appl. Surf. Sci.* **2016**, *374*, 96.